Nonlinear emission properties of an optically anisotropic GaN-based microcavity

Jacques Levrat,* Georg Rossbach, Amélie Dussaigne,† Gatien Cosendey, Marlene Glauser, Munise Cobet, Raphaël Butté, and Nicolas Grandjean
Institute of Condensed Matter Physics, École Polytechnique Fédérale de Lausanne, CH-1015 Lausanne, Switzerland

Henryk Teisseyre
Institute of High Pressure Physics, Polish Academy of Sciences, 01-142 Warsaw, Poland and
Institute of Physics, Polish Academy of Sciences, 02-668 Warsaw, Poland

Michał Boćkowski, Izabella Grzegory, and Tadeusz Suski
Institute of High Pressure Physics, Polish Academy of Sciences, 01-142 Warsaw, Poland
(Received 9 June 2011; revised manuscript received 27 July 2012; published 19 October 2012)

The pronounced optical in-plane anisotropy of a suitably designed nonpolar GaN-based microcavity, mainly inherited from the valence-band complexity of wurtzite semiconductors, allows the coexistence of two different light-matter coupling regimes along orthogonal polarization planes. When increasing the excitation power density, a transition to a nonlinear coherent emission is observed under nonresonant optical pumping for both polarization directions at carrier densities remaining well below the exciton-saturation level. Their differing nature is experimentally revealed by means of polarization-resolved Fourier space and near-field imaging. While one polarization direction exhibits all specificities of the strong light-matter coupling regime and features polariton lasing at high injection, the other one lacks a straightforward interpretation due to its complex coupling regime. Possible mechanisms are addressed and evaluated.

DOI: 10.1103/PhysRevB.86.165321 PACS number(s): 78.55.Cr, 71.36.+c, 42.55.Sa, 78.20.Fm

I. INTRODUCTION

In semiconductor microcavities (MCs), when the coupling strength between the cavity mode and active medium exceeds photon and exciton damping rates, the strong-coupling regime (SCR) takes place.[1] Then light-matter coupling is no longer perturbative and the new eigenmodes are the upper and lower polaritons (LP). In the low density limit, these quasiparticles behave as bosons[2] and polariton condensation is triggered when the ground-state occupancy reaches unity. The spontaneous decay of this macroscopic quantum state results in a nonlinear coherent emission often referred to as *polariton lasing*.[3] In the weak-coupling regime (WCR), where the Rabi oscillation period exceeds at least one of the bare mode lifetimes, an increase in the injected carrier density can also lead to nonlinear optical emission. If the corresponding threshold occurs above the exciton saturation density n_X^{sat}, Coulomb interaction is screened and lasing originates from an inverted electronic population. Conversely, for densities below n_X^{sat}, such a nonlinear emission could arise from excitonic enhancement of the optical gain and is referred to as *exciton lasing*. As for polariton lasing, the threshold is expected to be significantly lower than that of semiconductor photon lasers.[4]

The simultaneous observation of lasing emission in the WCR and SCR at the same sample position under steady excitation conditions cannot occur in structures exhibiting isotropic in-plane properties, e.g., GaAs,[5] CdTe,[6] and polar GaN MCs.[7] By contrast, in anisotropic MCs, variations in the bare cavity mode dispersion or the exciton optical response for different polarizations of light will in turn affect the way photons and excitons couple to each other.[8] Therefore such structures represent an ideal playground to investigate the impact of birefringence and/or exciton oscillator strength (f_{osc}) anisotropy on the light-matter coupling. Among the possible coupling regimes which can arise from the bare mode anisotropy, one might obviously expect to observe light emission either in the WCR or in the SCR for both directions.[8,9] Recently, room-temperature polariton lasing has been reported in an anisotropic organic MC, where orthogonal linearly polarized polariton branches were observed with lasing occurring at the bottom of the lowest energy mode.[9] Another unusual situation would take place when only one direction experiences the SCR. In such a case a peculiar polarization-dependent behavior resulting from different light-matter coupling regimes could be probed by collecting orthogonal planes of polarization of the emitted light, which is of interest since below n_X^{sat} it could allow the simultaneous observation of polaritonic and excitonic effects.

In this paper, the nonlinear emission properties of an anisotropic III-nitride MC are studied under nonresonant optical pumping. For one linear polarization direction the optical response shows unambiguous characteristics of the SCR and features the transition to polariton lasing when increasing the excitation power. The behavior monitored along the other polarization plane is more intricate: while lacking clear signatures of the SCR, nonlinear emission with comparable threshold is detected. To report on these aspects, the paper is organized as follows: In Sec. II important notes on the sample structure and experimental details are provided. Subsequently, we resume the linear optical properties of the investigated structure in Sec. III based on a previous publication (Ref. 10), which are further supported by additional transfer-matrix calculations accounting for the optical anisotropy. In Sec. IV we report on lasing in both polarization directions. Following the evidence of an exciton injection level well below the

Mott density, we conclude that polariton lasing occurs for one polarization direction, and discuss the possible origins of the nonlinear emission along the other one. Finally, we summarize our study and draw a conclusion in Sec. V.

II. SAMPLE DESIGN AND EXPERIMENTAL DETAILS

The present MC was grown by ammonia-based molecular beam epitaxy on a high quality *m*-plane bulk GaN substrate[11] and consists of a 50-pair $Al_{0.15}Ga_{0.85}N/Al_{0.35}Ga_{0.65}N$ bottom distributed Bragg reflector (bottom-DBR) followed by a 3λ $Al_{0.13}Ga_{0.87}N$ cavity containing five sets of 4 GaN quantum wells (QWs) with a thickness of 5 nm surrounded by 5-nm-thick barriers located at the antinodes of the electric field standing wave. The MC is completed by an eight-pair SiO_2/ZrO_2 top-DBR deposited by electron-beam evaporation. More structural information and a detailed investigation of the III-nitride layer stack can be found in Ref. 10.

To investigate the emission properties carriers were nonresonantly injected using a pulsed frequency-quadrupled Nd:YAG (yttrium aluminum garnet) laser (266 nm) with a repetition rate of 8.52 kHz and a pulse duration of 500 ps. The eigenmode dispersion is directly recorded by means of a Fourier-space imaging setup (far-field emission) using a UV microscope objective with a numerical aperture of 0.55, a spot area of $\sim 20\ \mu m^2$, and appropriate optics coupled to a liquid N_2-cooled UV-enhanced charge-coupled-device (CCD) monochromator combination with a spectral resolution $\sim 100\ \mu eV$. Real-space imaging is performed simultaneously by means of a nonpolarizing beam splitter and an extra high-resolution UV-enhanced CCD camera. For the angle-resolved reflectivity spectra the light of a 150 W Xe lamp was focused down to a $\sim 100\ \mu m$ diameter spot, collected with an angular resolution better than 1°, and guided through an optical fiber to the above-mentioned monochromator unit. Note further that all measurements and considerations throughout this paper refer to a temperature of $T = 50$ K [except for the reflectivity spectra displayed in Fig. 2(a)], which was reached by the use of a continuous-flow liquid-helium cryostat. This restriction arises from the limited matching between the excitons and the bottom-DBR stopband.[10]

III. LINEAR OPTICAL PROPERTIES

A. Basics: Light-matter coupling in the presence of optical anisotropy

In the presence of optical anisotropy the light-matter interaction constant g is affected by both the birefringence and the polarization-dependent oscillator strength (f_{osc}) distribution of the optically active excitons. Its magnitude corresponding to the exciton transition t and the electric-field polarization y is given by

$$g_y^t = \hbar \sqrt{\frac{e^2}{2\varepsilon_0 m_0} \frac{N_{\text{eff}}^{\text{QW}}}{n_{\text{cav},y} L_{\text{eff},y}} f_{\text{osc},y}^t}, \qquad (1)$$

where ε_0, m_0, and e represent the vacuum permittivity, the free electron mass, and its corresponding charge, respectively. $N_{\text{eff}}^{\text{QW}}$ denotes the number of QWs effectively coupled to the cavity mode.[12] Owing to the wells located slightly apart from the electric-field antinodes $N_{\text{eff}}^{\text{QW}}$ is reduced with respect to the geometrical value and amounts for the current structure to ∼16.3, meaning that three to four QWs over the 20 do not contribute to the light-matter interaction but act as an extra source of loss. Birefringence impacts on g via the averaged refractive index of the cavity n_{cav} and the effective cavity length L_{eff}. Depending on the cavity material, the influence of those quantities to the anisotropy of g is usually significantly lower than the impact of f_{osc}: In the (Al,Ga)N layers the relative variation in the refractive index along the two polarization directions amounts to ∼2% (cf. Table I).

TABLE I. Summary of the optical anisotropy inherited from the III-nitride layer stack with nonpolar surface orientation. The values for the bottom-DBR stopband position E_{DBR} and its spectral width ΔE_{SB} were taken from simulations.

	$n_{Al_{0.15}Ga_{0.85}N}$ ($E = 3.5$ eV)	$f_{\text{osc}}^{\text{rel,A}}$	$f_{\text{osc}}^{\text{rel,B}}$	E_{DBR} (eV)	ΔE_{SB} (meV)
$\mathbf{E} \parallel c$	2.625	0.74	0.26	3.55	100
$\mathbf{E} \perp c$	2.566	0.26	0.74	3.61	100

Consequently, the corresponding vacuum Rabi splitting Ω_{VRS} reads

$$\Omega_{\text{VRS},y}^t = 2 \cdot \mathbf{Re}\left\{\sqrt{\left(g_y^t\right)^2 - \frac{\gamma_{X,t}^2 + \gamma_{C,y}^2}{2}}\right\}, \qquad (2)$$

where $\gamma_{X,t}$ and $\gamma_{C,y}$ are the homogeneous linewidths of the excitonic transition X_t and the cavity mode in the y direction, respectively. Thus, in an anisotropic system it is obviously possible to promote one and the same excitonic transition into different coupling regimes with the independent photonic modes, primarily depending on the orientation of its dipole moment and to a lesser extent on the birefringence of the active region.

Note that for realistic systems featuring a certain degree of disorder another restriction due to the inhomogeneous linewidth has also to be considered. This is especially true for the exciton one $\gamma_{X,t}^{\text{inh}}$, which was shown to blur all characteristics of the SCR when it is exceeding $\Omega_{\text{VRS},y}^t$ and which is omnipresent in III-nitride heterostructures due to the small exciton Bohr radius and the correspondingly increased sensitivity to crystal imperfections and inhomogeneities.[13]

B. Optical response of the MC in the linear regime

The present MC structure exhibits a pronounced anisotropic optical response owing to the hexagonal symmetry of the wurtzite lattice and the nonpolar surface orientation. Indeed, the complex refractive index of III-nitrides corresponds to a uniaxial tensor with the optical axis parallel to the [0001] direction of the crystal (*c*-axis). Thus, incident light experiences different refractive indices when its electric field **E** is polarized parallel or perpendicular with respect to the *c*-axis. For the optical response of structures and devices with *c*-plane orientation, the commonly applied growth direction for III-nitride heterostructures, this anisotropy plays a minor role, since in this case the optical axis represents the normal to the sample surface. However, such so-called polar structures suffer from the quantum-confined Stark effect (QCSE),[14] where built-in electric fields arising from polarization discontinuities at

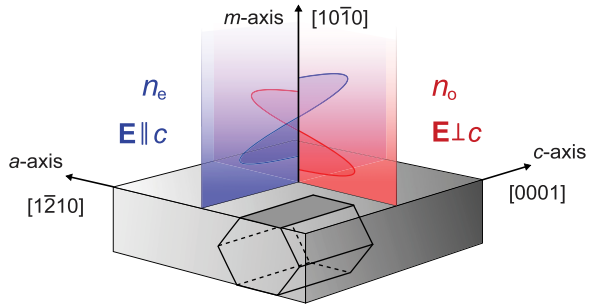

FIG. 1. (Color online) Schematic view of the m-plane crystal orientation and the corresponding anisotropic optical response.

heterostructure interfaces decrease the optical matrix elements and limit the efficiency of optoelectronic devices. These issues can be bypassed as a whole or in part when growing structures with non- or semipolar surface orientation,[15] respectively. Corresponding devices are therefore seen as promising candidates for the fabrication of efficient light-emitting diodes and laser diodes. With respect to exciton polaritons the enhanced radiative efficiency and the opportunity to use wider QWs due to the absence of QCSE is expected to favor the light-matter coupling strength.

The surface of the present nitride layer stack corresponds to a side facet of the hexagonal unit cell (m-plane), the optical axis lies in the surface plane, and the two components of the refractive index tensor are accessible along orthogonal polarization planes: $\mathbf{E} \perp c$ and $\mathbf{E} \parallel c$, denoted as the ordinary and extraordinary polarization direction (indices o and e), respectively. The situation is schematically depicted in Fig. 1. A detailed discussion on the linear optical properties of the current structure has been published elsewhere.[10] In summary, in accordance with the previous discussion two peculiarities have to be considered: the anisotropic f_{osc} distribution of the two contributing excitonic transitions X_{A} and X_{B}, and the optical birefringence leading to polarization-dependent energy shifts of the bottom-DBR stopband and the cavity mode. In the extraordinary direction the large f_{osc} of the low-energy exciton X_{A} ($E_{\mathrm{A}} \sim 3.55$ eV, $f^{\mathrm{A}}_{\mathrm{osc},o} : f^{\mathrm{A}}_{\mathrm{osc},e} = 0.26 : 0.74$) and the good overlap with the bottom DBR below 70 K lead to the appearance of the SCR between X_{A} and C_e with $\Omega^{\mathrm{A}}_{\mathrm{VRS},e} = 45$ meV. Figure 2 shows angle-resolved reflectivity and photoluminescence (PL) spectra for $\mathbf{E} \parallel c$ revealing a clear anticrossing signature of the lower polariton branch (LPB) with X_{A}. Furthermore, no signature of the upper polariton branch (UPB) or the SCR with X_{B} ($E_{\mathrm{B}} = E_{\mathrm{A}} + 15$ meV) can be identified. Regarding the UPB, the high excitonic fraction at small angles and the residual damping from the absorption tail of the continuum decrease its visibility with respect to the LPB and might conceal it below the noise level. The absence of the SCR with X_{B} can be explained by considering Eqs. (1) and (2) and the reduced oscillator strength of X_{B} ($f^{\mathrm{B}}_{\mathrm{osc},o} : f^{\mathrm{B}}_{\mathrm{osc},e} = 0.74 : 0.26$) along $\mathbf{E} \parallel c$, which results in an expected Rabi splitting of ~20 meV. The latter corresponds to the measured value of the exciton inhomogeneous linewidth γ^{inh}_X, which potentially leads to the disappearance of the SCR.[13] By contrast, for $\mathbf{E} \perp c$ no obvious evidence for the SCR could be traced for the two excitons; neither in reflectivity nor in PL (cf. Ref. 10). For X_{A} the weak oscillator strength

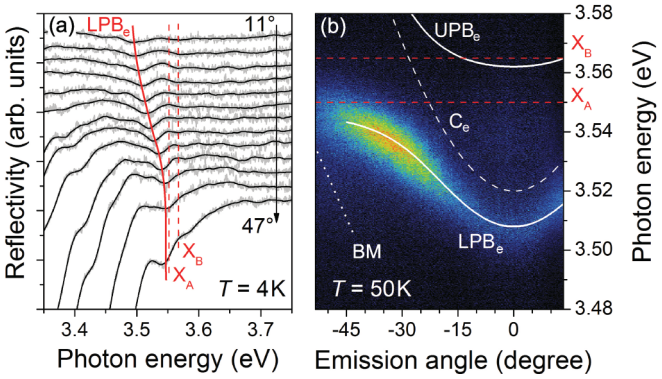

FIG. 2. (Color online) (a) Angle-resolved reflectivity spectra measured at 4 K with $\mathbf{E} \parallel c$: the red solid line acts as a guide to the eye for the LPB converging toward X_{A} at high angles (LPB$_e$). (b) Polarization-resolved Fourier-PL image acquired below threshold for $\mathbf{E} \parallel c$ at 50 K showing a clear anticrossing between LPB$_e$ and X_{A}, and a signature of the relaxation bottleneck.

allows one to draw the same conclusions as stated above for X_{B}. But X_{B} features a high oscillator strength along this direction, which should also result in the SCR presuming a good overlap with the bottom-DBR stopband. Since there is no straightforward interpretation, transfer-matrix simulations (TMS) have been performed in order to understand the intricate interplay between optical and excitonic anisotropies.

C. Anisotropic transfer-matrix simulations

TMS were carried out following the 4 × 4 matrix formalism of Schubert[16] and using anisotropic optical constants of AlGaN by linearly interpolating the experimental ones from GaN (Ref. 17) and AlN (Refs. 18 and 19) between 1 and 7 eV according to the analytic model of Shokhovets *et al.*[20] Thereby all imaginary parts have been neglected except for the QWs, for which the applied complex refractive index is displayed in Fig. 3(b). It consists of the two active excitonic transitions A and B, represented by a Voigt profile including the above-mentioned oscillator strength ratios, the corresponding band-to-band absorption edges separated by the exciton binding energy $E^B_X = 41$ meV as deduced from envelope function calculations and constituted of broadened sigmoid profiles, and a background refractive index dispersion. For the homogeneous and inhomogeneous linewidths values equal to $\gamma^{\mathrm{hom}}_X = 7$ meV and $\gamma^{\mathrm{inh}}_X = 20$ meV were adopted corresponding to the low injection case (cf. Fig. 8). Figure 3(a) shows the resulting cavity mode electric-field intensity distribution for the ordinary direction in the MC structure featuring different penetration lengths into the dielectric and the III-nitride DBRs as well as a pronounced overlap with the five QW sets.

The polarization-dependent TMS results for reflectivity, transmission, and absorption are displayed in Fig. 4. All spectra were calculated as a function of the external angle θ for s polarization, i.e., for a situation corresponding to unpolarized incident light and detection for the component perpendicularly polarized to the plane of incidence.

We first focus on $\mathbf{E} \parallel c$. As expected, an unambiguous signature of the SCR is observed between X_{A} and C_{e}. The LPB$_e$ mode converges toward X_{A} at high angles and moves

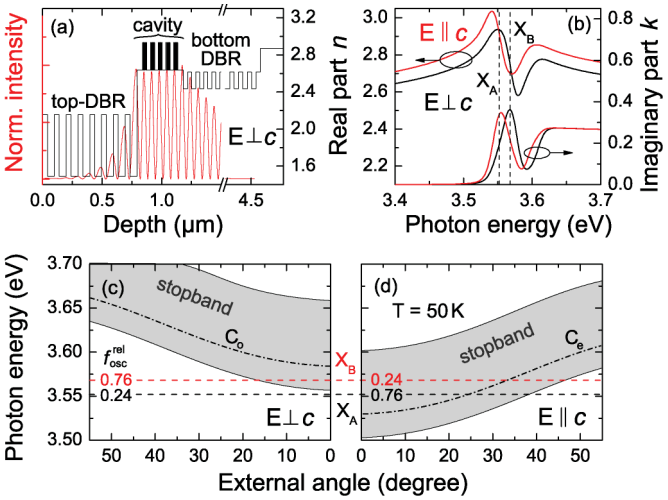

FIG. 3. (Color online) Optical properties of the studied MC structure: (a) depth profile of the refractive index at the cavity mode energy for $\mathbf{E} \perp c$ (black) and corresponding intensity profile of the electric field of light (red); (b) anisotropic complex refractive index of the QWs used for TMS; and (c) schematic view of the linear optical response for $\mathbf{E} \perp c$: The bottom-DBR stopband (gray) hardly overlaps with X_A and X_B, and the cavity mode C_o is expected to be positively detuned. (d) On the contrary, for $\mathbf{E} \parallel c$, there is a perfect overlap between the excitonic resonances and the bottom-DBR stopband, and the cavity mode C_e is slightly negatively detuned.

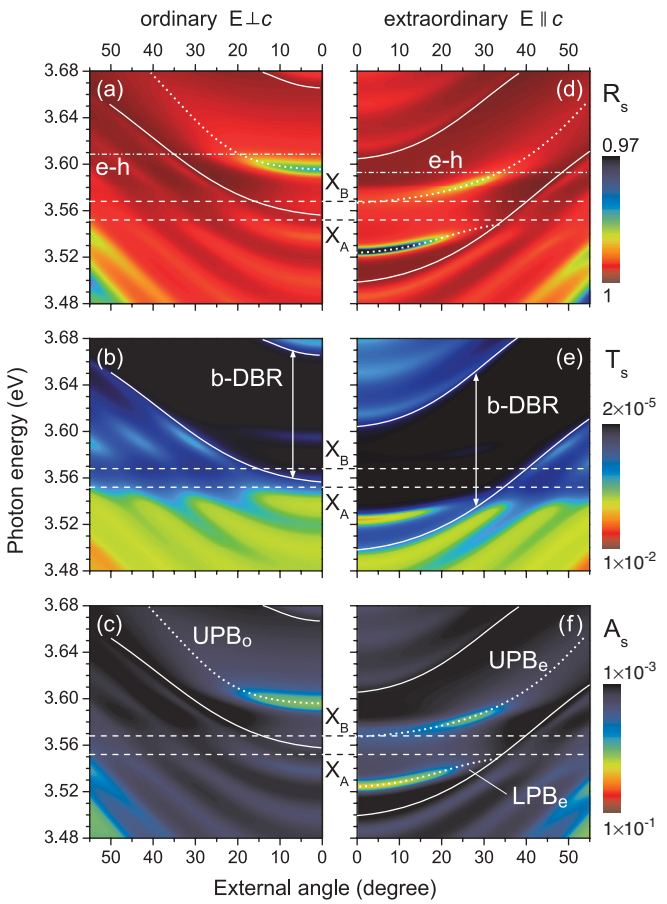

FIG. 4. (Color online) Results of anisotropic transfer-matrix simulations for the current structure: (a)–(c) reflectivity, transmission, and absorption spectra for the optical axis oriented parallel to the plane of incidence or $\mathbf{E} \perp c$, respectively, and (d), (e) for $\mathbf{E} \parallel c$. Horizontal dashed lines mark the energy position of the optically active excitons. In (a) and (d) the energy of the band-to-band absorption edges is also given [dash-dotted line, e–h]. In the transmission spectra the dispersive edges of the bottom DBR stopband are highlighted by continuous lines. Dotted lines act as a guide to the eye for apparent eigenmodes. Absorption and transmission maps are displayed in logarithmic scale. See text for details concerning the method and interpretation.

out of the bottom DBR stopband for $\theta > 35°$. For even higher angles a slight anticrossing with the bottom-DBR Bragg modes (BMs) can be identified. X_B is widely inapparent, which results from its small oscillator strength, the small energy splitting with X_A, and the comparably large broadening leading solely to a shoulderlike feature in the optical constants [cf. Fig. 3(b)]. Nevertheless, its presence is obvious from the large smearing of UPB_e close to $\theta = 0$ and the overall damping of the latter in reflectivity, an effect which is additionally enhanced by the proximity of the band-to-band absorption tail. In the end the minimum of the UPB_e reflectivity amounts to 0.985 around 27°, whereas the LPB_e dip goes down to 0.936 at $\mathbf{k}_\parallel = 0$. This result agrees well with the experimental findings of reflectivity shown in Fig. 2(a), where UPB_e does not emerge. Note that due to the relatively large spot size used for reflectivity measurements, which exceeds by far the scale of photonic disorder, a decreased sensitivity to corresponding dips is expected in general. Owing to the damping of UPB_e close to $\theta = 0$, while keeping in mind the analysis drawn in Ref. 10, the WCR is concluded for X_B along $\mathbf{E} \parallel c$. In the ordinary direction the situation is less obvious. The location of both excitons close to the low-energy stopband edge prohibits the formation of an eventual LPB_o mode. Nevertheless, it has been shown that one of the two polariton branches might exist without the other, e.g., when the UPB is damped by the band-to-band absorption.[21] Transferred to the present case, the absence of LPB_o owing to the weak photonic confinement does not automatically imply that UPB_o is also absent. Indeed, the conspicuous mode located at 3.595 eV might be ascribed to UPB_o, which is rapidly damped by the band-to-band absorption edge toward higher angles [Fig. 4(a)]. In line with this, an artificial redshift of the bottom-DBR position in the simulations reveals clear characteristics of the SCR between X_B and C_o (not shown here). However, the absence of a low-energy polaritonic mode is obvious and it will prevent the system from showing effects such as polariton lasing or condensation. Moreover, the presence of a weak reflectivity dip and a signature in absorption [cf. Figs. 4(a) and 4(c)] at the energy position of X_B at zero in-plane momentum ($\mathbf{k}_\parallel = 0$) suggests that the WCR is present. Note that this mode progressively transforms into LPB_o when redshifting the bottom-DBR stopband. For X_A, on the other hand, the same argumentation as mentioned for X_B along $\mathbf{E} \parallel c$ applies, i.e., its low oscillator strength is not sufficient to promote it into the nonperturbative regime due to the limitation set by the inhomogeneous broadening. The collective outcome from the sample anisotropy at $T = 50$ K obtained by means of TMS and experimental investigations in the linear regime are summarized in Figs. 3(c) and 3(d) and in Table I.

IV. NONLINEAR EMISSION PROPERTIES

In this section, the polarization-dependent emission properties of the present MC under nonresonant optical pumping are studied. Lasing is observed for both polarization directions emerging well below the exciton saturation level with different threshold power densities $P_{\mathrm{thr},e}$ and $P_{\mathrm{thr},o}$ along extraordinary and ordinary directions, respectively.

A. Injection-dependent far-field imaging

In Figs. 5(a)–5(c), the evolution of the far-field emission is reported for three different pump power densities at $T = 50$ K. No polarization selection was set in the collection line so that both polarization components $\mathbf{E} \parallel c$ and $\mathbf{E} \perp c$ are detected.

In the low injection regime [Fig. 5(a), average power density $P = 7\ \mathrm{W/cm^2}$] the spectrum is dominated by a broad emission band around 3.535 eV, which is restricted to small angles and features a slightly dispersive shape. On its low-energy side another mode emerges, narrower and more dispersive, that converges toward X_{A} at higher angles (see also Fig. 2). In accordance with the results of Ref. 10 and Fig. 2 we assign it to LPB_e. The origin of the other mode can be understood by considering the existence of exciton localization at such low temperature and injection. Indeed, excitons not coupled to C_e, either due to the selection rules or the partly uncoupled QWs located slightly apart from the cavity light field antinodes, relax in the local disorder landscape and thus emit light at an energy lowered by the localization energy $E_{\mathrm{loc}} \sim 15$ meV.[10] They are allowed to escape from the cavity via the finite DBR reflectivity, the dark exciton modes in the presence of disorder,[22] or most likely the first low-energy BM in the ordinary direction as revealed by TMS visible in Figs. 4(a)–4(c). The latter mechanism does also explain the slightly dispersive shape and the restriction to small external angles. For low injection these photons mainly originate from localized states of the A exciton $X_{\mathrm{A,loc}}$.

Increasing further the excitation power results at $P = P_{\mathrm{thr},e} = 15\ \mathrm{W/cm^2}$ in a nonlinear increase in the LPB_e emission intensity around $\theta = 0$ and the appearance of a third mode L_o at higher energy ($E_{L,o} = 3.552$ eV), whose physical origin is not obvious from TMS and that will be discussed in Sec. IV C. The latter also exhibits a transition toward a nonlinear emission regime for a higher pump power density: $P_{\mathrm{thr},o} \approx 1.3 P_{\mathrm{thr},e}$. This lasing feature is more apparent in the polarization-resolved power series measured at zero in-plane momentum presented in Fig. 6(b). For $\mathbf{E} \perp c$, the low injection regime is dominated by the $X_{\mathrm{A,loc}}$ emission leaking out through the first low-energy BM. An increase in the excitation power induces a progressive blueshift of the emission line accompanied with the rise in the L_o occupancy, either by delocalization of excitons or by occupation of $X_{\mathrm{B,loc}}$ states. Lasing emission from the L_o mode occurs energetically between the free excitons X_{A} and X_{B} with a linewidth of $\sim$2.5 meV at threshold. Note that LPB_e is completely absent along this polarization direction. This counter-polarization of LPB_e with respect to $X_{\mathrm{A,loc}}$ and L_o and the corresponding unique anisotropic light-matter coupling regime in the present structure is emphasized by the angle-integrated ($-33^\circ < \theta < 33^\circ$) polarization series presented in Fig. 6(a), which was recorded above the two nonlinear emission thresholds. Accordingly, for polarization $\mathbf{E} \parallel c$ the light emission is dominated by LPB_e for all excitation power densities. Note that the linewidths of both counter-polarized lasing emissions are lower than the bare cavity mode one ($\sim$10 meV), which is a fingerprint of temporal coherence. In addition it is worth mentioning that along the extraordinary direction the signature of localized exciton states is much weaker [or even negligible depending on the sample spot; cf. Figs. 2 and 6(a)] although the oscillator strength of X_{A} is maximum.[23] Here, it solely emerges from partially uncoupled QWs (dark excitons), as the localization of strongly coupled excitons is inhibited by the fast Rabi oscillations.[24]

From the measurements shown in Fig. 5 and the corresponding injection-dependent analysis displayed in Fig. 7, it is obvious that the nonlinear emission first occurs slightly above the bottom of LPB_e but well below C_e for an average threshold power density $P_{\mathrm{thr},e} \approx 15\ \mathrm{W/cm^2}$ and then at L_o for a slightly higher power density. The first one displays typical features of polariton lasing that are a nonlinear increase in the intensity at $\mathbf{k}_{\parallel} = 0$ due to final-state stimulation, a blueshift of the emission due to polariton-polariton interactions and oscillator strength saturation,[25] and a narrowing of the emission line from 15 down to 1 meV [Figs. 7(a) and 7(b)], which reflects the increase in the coherence time following the spontaneous

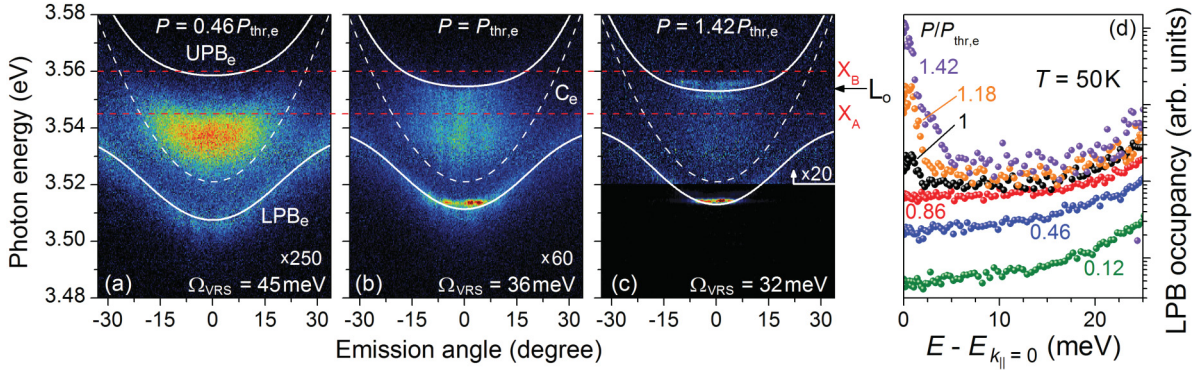

FIG. 5. (Color online) (a)–(c) Fourier images measured at various excitation power densities below and above the polariton lasing threshold ($P_{\mathrm{thr},e}$) without polarization selection at $T = 50$ K. Fitted coupled modes (white solid lines) are displayed for $\mathbf{E} \parallel c$ only. The two free exciton lines (red) are active in both directions. (d) LPB occupancy as a function of excitation power.

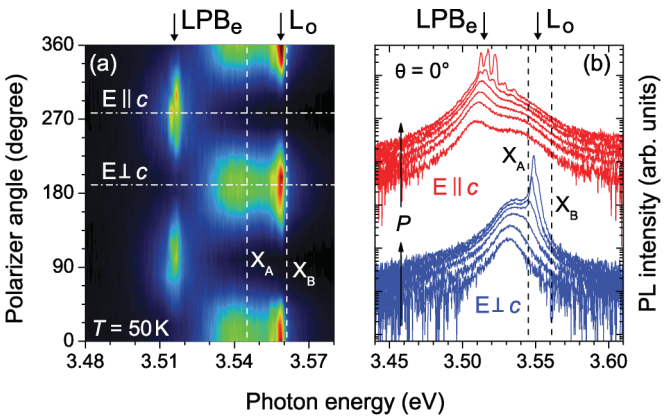

FIG. 6. (Color online) Polarization-resolved photoluminescence measurements performed at 50 K: (a) angle-integrated far-field spectra ($-33^\circ < \theta < 33^\circ$) recorded above $P_{\mathrm{thr},e}$ and $P_{\mathrm{thr},o}$ as a function of the polarizer angle and (b) spectra at normal incidence as a function of the excitation power density P ranging from 0.07 to $2.14P_{\mathrm{thr},e}$ for $\mathbf{E} \parallel c$ (red) and $\mathbf{E} \perp c$ (blue). The spectra for $\mathbf{E} \parallel c$ are vertically shifted for the sake of clarity.

buildup of a polariton condensate. Similarly to measurements performed on a c-plane GaN multiple QW-based MC,[26] the vacuum Rabi splitting is reduced from 45 down to 32 meV over the investigated power range likely due to saturation of the exciton oscillator strength. However, the polariton emission remains below the C_e energy for all applied excitation power densities ensuring that the system remains in the SCR. Finally, it is worth pointing out that the nonthermal occupancy of LPB$_e$ shown in Fig. 5(d), likely arises from the limited quality factor $Q \approx 350$ and the reduced polariton relaxation efficiency for negative detunings in combination with the low temperature.[26,27]

B. Evidencing an injection below the Mott density

To further confirm our assumption that the electronic population is dominated by excitons, we will now demonstrate that the system operates below the exciton saturation density n_X^{sat} for all power densities explored. In a strongly coupled system, it is commonly accepted to relate the LPB blueshift to the exciton density n_X via the relationship $\Delta E_{\mathrm{LPB}} = 6n_X a_B^2 E_X^B |X_0|^2$, where a_B denotes the effective Bohr radius of

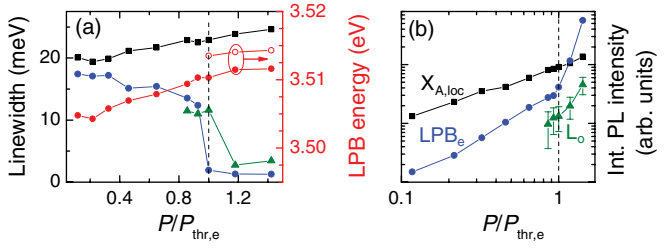

FIG. 7. (Color online) Analysis of the excitation power-dependent eigenmode profiles at $\mathbf{k}_\parallel = 0$: (a) linewidth evolution of the LPB$_e$ (blue circles), $X_{\mathrm{A}}^{\mathrm{loc}}$ (black squares), and L_o (green triangles) and the photon energy of the linear (red solid circles) and nonlinear (red open circles) LPB$_e$ emissions; and (b) evolution of the corresponding integrated PL intensities.

the QW exciton, E_X^B is the exciton binding energy, and $|X_0|^2$ and ΔE_{LPB} are the excitonic fraction and the LPB energy shift at zero in-plane momentum, respectively.[25] However, this treatment is only valid provided the LPB renormalization can be exclusively attributed to exciton-exciton interactions, which is not the case for GaN-based systems where the oscillator strength saturation cannot be neglected, even below the polariton lasing threshold.[26] This leads to a significant overestimate of n_X resulting for the present structure in an injection density approximately twice the saturation level deduced in Ref. 28, i.e., $n_X^{\mathrm{sat}} \sim 1.3 \times 10^{12}$ cm^{-2}. Indeed, the impact of saturation effects is revealed by the observation of a Ω_{VRS} reduction by ~30% for the injection range investigated (see Fig. 5). In addition, the renormalization analysis is made more complex since the lasing mode is slightly blueshifted with respect to the bottom of LPB$_e$ [see Figs. 5(b) and 7(a)], likely due to photonic disorder.[7,29]

A more reliable way to compare n_X with n_X^{sat} first consists in investigating the optical response of the bare active medium as a function of the injected carrier density for the same excitation conditions. From the power-dependent PL series performed on the half-MC at the same temperature, $T = 50$ K [see Fig. 8(a)], it is seen that the QW emission linewidth decomposed into homogeneous and inhomogeneous contributions [Fig. 8(c)] shows a singular behavior at $P_{\mathrm{crit}} \approx 140$ W/cm^2 where the rise in the homogeneous broadening becomes much faster.[30] For $P < P_{\mathrm{crit}}$ the moderate increase in the homogeneous linewidth can be ascribed to carrier heating induced by collisions, whereas the fast rise in the carrier temperature and the transition to an exponentially decaying slope for the high-energy tail when $P > P_{\mathrm{crit}}$ can be attributed to a progressive loss of the excitonic character—the Mott transition, compliant with Ref. 31. According to Fig. 8(b) the effective electron-hole plasma temperature at P_{crit} amounts to ~180 K, which remains well below the exciton cut-off temperature given by E_X^B and still ensures the exciton stability. Thus P_{crit} represents the lower limit of the Mott-transition onset, although an earlier rise of the exponential decay might be hidden by the large linewidth. Note that this transition continuously occurring above P_{crit} should be accompanied with an emission energy redshift due to band-gap renormalization. This effect is hardly observable in GaN-based MCs (polar and nonpolar ones): First, due to the large number of QWs, when increasing the power density the Mott transition is initially passed in the QWs closest to the surface, while the rest of them remain below the critical density. This explains the simultaneous observation of luminescence from excitons and the electron-hole plasma for high power densities in Fig. 8(a) and will hide small redshifts of the plasma emission. Second, this redshift might be partially compensated by a blueshift caused by the progressive exciton screening.

To transpose this discussion to the full-MC case the power density of the polariton lasing threshold $P_{\mathrm{thr},e}$ is also reported in Fig. 8(c) by a vertical red-dashed line lying about one order of magnitude below P_{crit}. Note that this position with respect to the Mott transition states an upper limit only. In the full-MC the different surface reflectivity, the transmission of the top-DBR at the pump wavelength (~65%), and the redistribution of the radiative excitons inside the cavity section have to be considered. Indeed, whereas in the half-MC only the

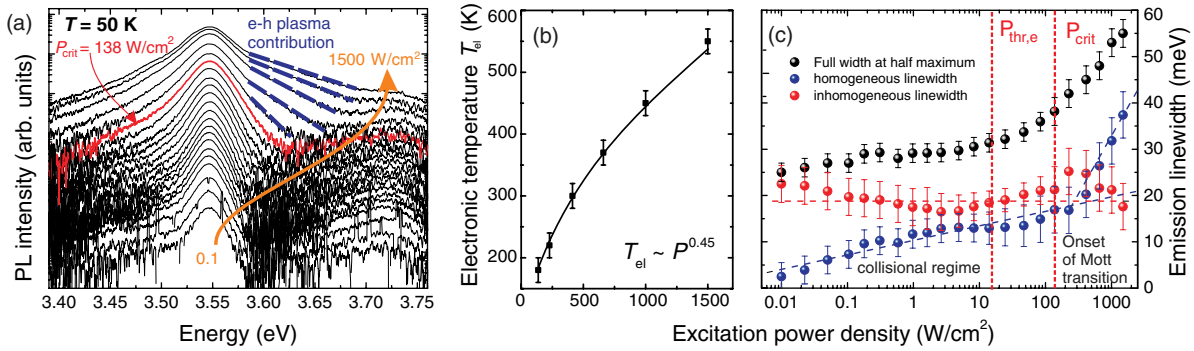

FIG. 8. (Color online) (a) Excitation power-dependent emission spectra taken on the half-MC without top-DBR at $T = 50$ K without polarization selection. Evolution of (b) the electron-hole plasma effective temperature (T_{el}) and (c) the QW emission linewidth deduced from a Voigt-profile analysis.

first set of four QWs is significantly populated due to the strong absorption at the pumping wavelength, the optical feedback in the full-MC leads to a fast redistribution of the carriers coupled to the cavity light field by emission and reabsorption processes (Rabi oscillations) and thus to a lower exciton density per QW. Note that it only applies for exciton polaritons possessing a significant photonic fraction, i.e., the excitonic reservoir does not take directly part to the light-matter interaction and decays with the nonradiative exciton lifetime τ_X^{NR}.

According to experiments, where no significant changes in the emission characteristics of the full-MC are observed [cf. exciton linewidth evolution shown in Fig. 7(a)], the preservation of a subsaturation carrier density and thus the SCR for the whole injection regime investigated in this work is ensured. Considering the relatively low lattice temperature and the high exciton binding energy, free and localized excitons dominate the optical response of the QWs and the contribution of thermal free electrons can be considered as negligible.[32]

C. Possible origins of the lasing action in the ordinary direction

Having confirmed an injected carrier density below the exciton saturation level and correspondingly concluded that polariton lasing is appearing for the extraordinary polarization direction, the specificities of the L_o mode shall be addressed in the current section—in particular, its photonic origin and the mechanism of *gain* driving the nonlinear emission.

Conventional lasing in a semiconductor structure can only emerge when the excitonic resonance is screened and gain is provided by an inverted electron-hole population, i.e., at an injection level higher than the Mott density.[33] According to the previous discussion, lasing based on the Bernard-Duraffourg condition can thus be safely excluded for L_o. Nevertheless, in a system operated below the exciton saturation level a nonlinear emission can still occur either due to the spontaneous decay of a coherent polariton condensate as evidenced for $\mathbf{E} \parallel c$ or alternatively be issued from so-called *excitonic gain*. As an exciton represents a simple two-level system, the latter mechanism requires the involvement of an additional mechanism such as a biexcitonic[34] or phonon-assisted transition,[35] bosonic condensation of excitons,[36] an efficient exciton-exciton scattering channel,[37,38] or a third level induced by the presence of localized excitonic states.[4] Those mechanisms shall be briefly addressed in the following.

According to the Haynes rule[39] we conclude that the biexciton binding energy does not exceed 10 meV for the thick QWs used in the present structure. Owing to the comparably larger inhomogeneous linewidth and the absence of any biexciton signature for the whole injection regime explored [cf. Fig. 8(a)] we exclude biexciton-related excitonic gain as lasing origin.

Both the phonon-assisted transition and the exciton-exciton scattering mechanism following Hvam[38] can be easily ruled out as gain source since the energy position of the lasing emission L_o is located between X_A and X_B. Indeed, with an LO-phonon energy of 92 meV and $E_X^B = 41$ meV the corresponding nonlinear emission would be expected to emerge considerably below the exciton resonances.

Bosonic condensation appears when the particle wave-function extent reaches the interparticle distance: According to their effective mass this is expected to occur only at temperatures as low as 1 K for excitons[36] and thus cannot be responsible for the present lasing feature.

The gain mechanisms described by Jen *et al.*[37] and Ding *et al.*[4] rely on the presence of localized exciton states manifesting themselves in a mainly inhomogeneous linewidth. In both cases gain emerges around the energy of the localized excitons, i.e., at the free exciton energy reduced by E_{loc}. However, the underlying mechanism appears to be different. Whereas Jen *et al.* observed a gain redshift with increasing power density and describe this effect in the framework of inelastic exciton-exciton scattering events occurring within the localized exciton population, the model introduced by Ding *et al.* predicts a gain blueshift.[4] This is justified by a theory of gain arising from saturated localized states in the low-energy tail of the exciton emission. Transferred to the present case, these mechanisms exclude the involvement of $X_{A,loc}$ states due to the higher energy of L_o. Nevertheless, the energy position of L_o coincides with $X_{B,loc}$, which features a higher radiative efficiency along this polarization direction due to the high f_{osc} of X_B and which is filled subsequently to the saturation of the $X_{A,loc}$ states. The eventual gain band will cover the full $X_{A,loc}$ and $X_{B,loc}$ range giving rise to a nonlinear emission occurring at the energy position exhibiting the largest optical feedback. The latter is heavily depending on the question of the coupling

regime along the ordinary polarization direction and thus the position of the bottom-DBR stopband, which is in favor of lasing on $X_{B,loc}$.

As stated in Sec. III C on the basis of TMS, no straightforward conclusion can be drawn for the coupling regime of X_B for $\mathbf{E} \perp c$ due to the limited optical confinement by the bottom-DBR stopband, while X_A is expected to be weakly coupled. Experimentally, L_o appears ~40 meV above LPB_e between the X_A and X_B free excitons. An identification with UPB_o, i.e., the dispersive photonlike mode at 3.595 eV determined by TMS [cf. Figs. 4(a)–4(c)], can thus be safely excluded by its energy position. According to the TMS results the weak mode emerging around zero in-plane momentum close to X_B appears more probable. As stated in Sec. III C it originates from the LPB_o due to the drastically reduced optical confinement and coupling strength thus providing only a very lossy optical feedback. At this stage it is important to explicitly point out that the optical constants of AlGaN used for TMS were obtained by a linear interpolation between those of GaN and AlN and do not necessarily perfectly coincide with those of the real structure, although they are reproducing the experimental findings quite well. According to Table I the relative anisotropy for the applied optical constants of $Al_{0.15}Ga_{0.85}N$ amounts to ~2.3% at 3.5 eV. A reduced value would cause a redshift of the ordinary cavity mode C_o, which could finally be at an energy position identical to L_o for a relative anisotropy of ~1.3% neglecting the influence of X_B. With an analogous reasoning L_o could also represent the first low-energy BM of the bottom-DBR. Those last two interpretations would additionally explain the dispersive shape especially visible in the far-field image of Fig. 9(e).

The interpretation in terms of lasing relying on localized states is further supported by the polarization-dependent real-space emission patterns shown in Fig. 9. Whereas the emission profile below $P_{thr,e}$ is unstructured and corresponds to that of the pump spot, the patterns measured above $P_{thr,o}$ reveal the different nature of the lasing mechanisms. For light emitted along $\mathbf{E} \parallel c$ the nonlinear increase in intensity occurs at the bottom of LPB_e [Fig. 9(d)] and the near-field emission pattern exhibits randomly distributed emission hot spots even apart from the center of the pump spot. They correspond to polariton traps induced by photonic disorder in agreement with the broadening observed in momentum space.[26,29] Conversely, for $\mathbf{E} \perp c$ in Fig. 9(c), the nonlinear emission exclusively arises from a small region close to the maximum pump power density as expected for lasing action occurring in the weak-coupling regime, where stimulated emission is triggered when the gain exceeds the losses. It is worth recalling that despite their distinct nature both nonlinear emissions emerge from the same spot and thus coexist and share the same exciton reservoir. Thus, we can rule out a situation similar to what has been reported by Lagoudakis *et al.*,[40] where the SCR and WCR simultaneously exist spatially separated due to an inhomogeneous pump spot. Finally, polariton lasing cannot be completely discarded as possible lasing origin for $\mathbf{E} \perp c$ from the real-space emission pattern only. Due to the reduced coupling strength and the proximity to X_B, polaritons would be very excitonlike and thus insensitive to the photonic disorder landscape and limited in motion by the exciton diffusion length. Both effects are in agreement with the strong emission

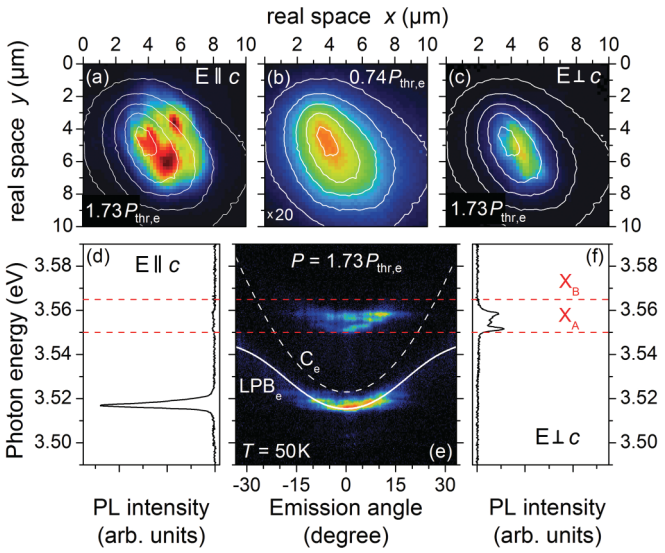

FIG. 9. (Color online) (e) Fourier space image measured above the two lasing thresholds without polarization selection (logarithmic color scale, $T = 50$ K). (d), (f) Polarization-resolved spectral profiles at $\mathbf{k}_\parallel = 0$. (a), (c) Color maps of the corresponding polarization-resolved near-field images. The superimposed white solid lines represent the near-field emission pattern measured below threshold without polarization selection displayed in (b).

occurring close to the maximum pump intensity. Nevertheless, the shallow LPB trap and the high density of states would cause a drastically increased polariton lasing threshold inconsistent with the observed behavior.[27]

The observed proximity between $P_{thr,e}$ and $P_{thr,o}$ looks surprising as polariton lasing is often claimed to be an ultralow threshold mechanism owing to the light effective mass of polaritons and the release of the Bernard-Duraffourg condition. Nevertheless we recall that the threshold is limited by the carrier relaxation kinetics and the finite lifetime of the exciton reservoir resulting in a significantly increased threshold with respect to the optimum case set by the thermodynamics.[27] The out-of-equilibrium nature of the presently observed polariton condensation is confirmed by the nonthermal occupancy of LPB_e in Fig. 5(d). Another important aspect, which could explain the proximity between the two thresholds, is that a lasing mechanism relying on localized states would depend on a zero- and not a two-dimensional density of states resulting in a low threshold to reach the transparency condition on X_B^{loc}. Finally the observation of a randomly distributed $P_{thr,o}/P_{thr,e}$ ratio, which ranges between 0.8 and 5 (data not shown) all over the sample indicates that the lasing mechanism involved for $\mathbf{E} \perp c$ strongly depends on the local excitonic and photonic disorder landscapes, which both affect the system losses. In any case, at this stage a quantitative comparison between the two thresholds remains rather elusive and a detailed understanding of the lasing mode in the ordinary direction still awaits further theoretical developments and experimental evidence. A comprehensive determination of the excitonic gain curve and the understanding of the corresponding lasing emission is prevented by the large uncertainties on the homogeneous and inhomogeneous line shapes, the localization center density, the

origin of the optical feedback and the corresponding losses, the injected carrier densities, and the limited knowledge about the anisotropic optical constants. Thus, in order to firmly assess the excitonic origin of the observed nonlinearities for $\mathbf{E} \perp c$, supplementary investigations are required. In particular, optical gain measurements should be performed and the presence of a second threshold when the system transits toward a degenerate electron-hole plasma should be observed above the Mott transition. However, it is worth mentioning that the high exciton binding energy and the important disorder in III-nitride compounds suggest that gain associated to localized states might occur. As an illustration, Kojima and co-workers have reported gain of two different origins in InGaN-based QW laser diodes.[41] Interestingly, for the device presenting the largest inhomogeneous broadening, they observed gain on the low-energy side of the absorption profile which was rapidly saturated for larger injection densities at the expense of the main transition peak. Hirano and Kanemitsu have also reported on the presence of a second gain mechanism below the band edge and ascribed it to localized excitons.[42] These observations are consistent with the phase-space filling model of Ding *et al.*,[4] and the rapid saturation of the gain can be ascribed to the reduced density of localized states compared to free ones. As the present structure relies on GaN QWs, the degree of disorder is lower compared to their InGaN counterparts. Nevertheless, at $T = 50$ K localization is still expected to play a dominant role in this system. Note finally that gain on the exciton transition without population inversion would also be possible if the coherence length of carriers is comparable to the device dimensions. In this case, the system can switch to a superradiant state resulting in an intense pulsed spontaneous emission of radiation.[43]

V. CONCLUSION

In conclusion, optical and excitonic anisotropy in the present nonpolar III-nitride MC create a unique polarization coupling regime: The extraordinary direction shows all characteristics of the SCR, while along the ordinary polarization direction a clear distinction between SCR and WCR is hampered by the weak optical confinement. Nevertheless, when increasing the nonresonant optical pump intensity nonlinear coherent emissions with distinct thresholds, originating from the same sample spot and thus a shared carrier population, are observed for both coupling regimes for a carrier injection well below the Mott density. Polarization-resolved Fourier-plane and near-field imaging measurements allow one to unambiguously ascribe the emission emerging in the extraordinary polarization direction to polariton lasing. The origin of lasing along the other direction is less obvious: After a careful consideration of all possible mechanisms, excitonic gain based on saturation of localized states appears to be the most likely mechanism but requires further validation.

In the end, such MC structures provide new perspectives for the study of nonpolar III-nitride light emitters, which exhibit both an enhanced efficiency owing to the absence of the QCSE[15] and an intrinsically linearly polarized light emission making such structures ideally suited for applications where the latter is essential, e.g., LCD screens. Moreover, we wish to emphasize that the coexistence of excitons undergoing different coupling regimes should be suitable for the realization of efficient stimulated emitters of THz radiation owing to a recent theoretical proposal.[44] Finally, anisotropic microcavities represent a unique tool to tailor the light-matter coupling regime and open new perspectives for investigating the physics of excitonic nonlinearities occurring in confined semiconductor systems.

ACKNOWLEDGMENTS

This work was supported by the NCCR Quantum Photonics, a research instrument of the Swiss National Science Foundation (SNSF), by the SNSF (Grant No. 200020-113542), by the EU-project Clermont4 (Grant No. FP7-235114), and by the European Regional Development Fund (grant Innovative Economy—POIG.01.01.02-00-008/08).

*jacques.levrat@epfl.ch

†Present address: CEA-LETI, Minatec Campus, 38054 Grenoble, France.

[1] C. Weisbuch, M. Nishioka, A. Ishikawa, and Y. Arakawa, Phys. Rev. Lett. **69**, 3314 (1992).

[2] M. Kira, F. Jahnke, S. W. Koch, J. D. Berger, D. V. Wick, T. R. Nelson, G. Khitrova, and H. M. Gibbs, Phys. Rev. Lett. **79**, 5170 (1997).

[3] A. Imamoğlu, R. J. Ram, S. Pau, and Y. Yamamoto, Phys. Rev. A **53**, 4250 (1996).

[4] J. Ding, H. Jeon, T. Ishihara, M. Hagerott, A. V. Nurmikko, H. Luo, N. Samarth, and J. Furdyna, Phys. Rev. Lett. **69**, 1707 (1992).

[5] D. Bajoni, P. Senellart, E. Wertz, I. Sagnes, A. Miard, A. Lemaître, and J. Bloch, Phys. Rev. Lett. **100**, 047401 (2008).

[6] Le Si Dang, D. Heger, R. André, F. Boeuf, and R. Romestain, Phys. Rev. Lett. **81**, 3920 (1998).

[7] S. Christopoulos, G. B. H. von Högersthal, A. J. D. Grundy, P. G. Lagoudakis, A. V. Kavokin, J. J. Baumberg, G. Christmann, R. Butté, E. Feltin, J.-F. Carlin *et al.*, Phys. Rev. Lett. **98**, 126405 (2007).

[8] M. Litinskaya, P. Reineker, and V. M. Agranovich, Phys. Status Solidi A **201**, 646 (2004).

[9] S. Kéna-Cohen and S. R. Forrest, Nat. Photonics **4**, 371 (2010).

[10] G. Rossbach, J. Levrat, A. Dussaigne, G. Cosendey, M. Glauser, M. Cobet, R. Butté, N. Grandjean, H. Teisseyre, M. Bockowski *et al.*, Phys. Rev. B **84**, 115315 (2011).

[11] H. Teisseyre, J. Z. Domagala, B. Lucznik, A. Reszka, B. J. Kowalski, M. Bockowski, G. Kamler, and I. Grzegory, Appl. Phys. Express **5**, 011001 (2011).

[12] V. Savona, L. C. Andreani, P. Schwendimann, and A. Quattropani, Solid State Commun. **93**, 773 (1995).

[13] G. Christmann, R. Butté, E. Feltin, J.-F. Carlin, and N. Grandjean, Phys. Rev. B **73**, 153305 (2006).

[14]M. Leroux, N. Grandjean, J. Massies, B. Gil, P. Lefebvre, and P. Bigenwald, Phys. Rev. B **60**, 1496 (1999).
[15]P. Waltereit, O. Brandt, A. Trampert, H. T. Grahn, J. Menniger, M. Ramsteiner, M. Reiche, and K. H. Ploog, Nature (London) **406**, 865 (2000).
[16]M. Schubert, Phys. Rev. B **53**, 4265 (1996).
[17]C. Buchheim, M. Röppischer, R. Goldhahn, G. Gobsch, C. Cobet, C. Werner, N. Esser, A. Dadgar, M. Wieneke, J. Bläsing *et al.*, Microelectron. J. **40**, 322 (2009).
[18]G. Rossbach, M. Röppischer, P. Schley, G. Gobsch, C. Werner, C. Cobet, N. Esser, A. Dadgar, M. Wieneke, A. Krost *et al.*, Phys. Status Solidi B **247**, 1679 (2010).
[19]G. Rossbach, M. Feneberg, M. Röppischer, C. Werner, N. Esser, C. Cobet, T. Meisch, K. Thonke, A. Dadgar, J. Bläsing *et al.*, Phys. Rev. B **83**, 195202 (2011).
[20]S. Shokhovets, R. Goldhahn, G. Gobsch, S. Piekh, R. Lantier, A. Rizzi, V. Lebedev, and W. Richter, J. Appl. Phys. **94**, 307 (2003).
[21]S. Faure, T. Guillet, P. Lefebvre, T. Bretagnon, and B. Gil, Phys. Rev. B **78**, 235323 (2008).
[22]P. Corfdir, J. Levrat, G. Rossbach, R. Butté, E. Feltin, J.-F. Carlin, G. Christmann, P. Lefebvre, J.-D. Ganière, N. Grandjean *et al.*, Phys. Rev. B **85**, 245308 (2012).
[23]Note that the polarization properties of localized exciton states can be altered with respect to the free ones depending on the spatial dimension and the symmetry of the localization center (Refs. 45 and 46). However, results of Ref. 10 suggest that in the present structure unpolarized defect states only contribute marginally at very low temperature and the majority of localized excitons follows the selection rules of the free ones.
[24]The localization time of excitons in a QW τ_{loc} is long compared to the Rabi period $\tau_{\mathrm{Rabi}} = \frac{2\pi\hbar}{\Omega_{\mathrm{VRS}}} < 100$ fs. For high quality nonpolar bulk GaN layers with a carrier density of 10^{16} cm^{-3}, τ_{loc} amounts to $\sim$25 ps for X_{A} and X_{B} at 8 K (Ref. 47). For QWs, this time is likely shorter due to in-plane disorder but a value larger than 100 fs is expected (Ref. 48).
[25]C. Ciuti, P. Schwendimann, B. Deveaud, and A. Quattropani, Phys. Rev. B **62**, R4825 (2000).
[26]R. Butté, J. Levrat, G. Christmann, E. Feltin, J.-F. Carlin, and N. Grandjean, Phys. Rev. B **80**, 233301 (2009).
[27]J. Levrat, R. Butté, E. Feltin, J.-F. Carlin, N. Grandjean, D. Solnyshkov, and G. Malpuech, Phys. Rev. B **81**, 125305 (2010).
[28]G. Christmann, R. Butté, E. Feltin, A. Mouti, P. A. Stadelmann, A. Castiglia, J.-F. Carlin, and N. Grandjean, Phys. Rev. B **77**, 085310 (2008).
[29]M. Richard, J. Kasprzak, R. André, R. Romestain, L. S. Dang, G. Malpuech, and A. Kavokin, Phys. Rev. B **72**, 201301 (2005).
[30]In the deconvolution procedure, only the contribution of X_{A} is considered due to the small occupancy of X_{B} states at such low lattice temperature. However, the progressive filling of X_{B} will likely result in an asymmetric line shape, which is blurred by the electron-hole contribution at large power densities.
[31]L. Kappei, J. Szczytko, F. Morier-Genoud, and B. Deveaud, Phys. Rev. Lett. **94**, 147403 (2005).
[32]P. Tsotsis, P. S. Eldridge, T. Gao, S. I. Tsintzos, Z. Hatzopoulos, and P. G. Savvidis, New J. Phys. **14**, 023060 (2012).
[33]H. Hanamura and H. Haug, Phys. Rep. **33**, 209 (1977).
[34]F. Kreller, M. Lowisch, J. Puls, and F. Henneberger, Phys. Rev. Lett. **75**, 2420 (1995).
[35]Y. Kawakami, I. Hauksson, J. Simpson, H. Stewart, I. Galbraith, K. A. Prior, and B. C. Cavenett, J. Cryst. Growth **138**, 759 (1994).
[36]L. V. Butov, C. W. Lai, A. L. Ivanov, A. C. Gossard, and D. S. Chemla, Nature (London) **417**, 47 (2002).
[37]J. Y. Jen, T. Tsutsumi, I. Souma, Y. Oka, and H. Fujiyasu, Jpn. J. Appl. Phys. **32**, L1542 (1993).
[38]J. M. Hvam, Solid State Commun. **12**, 95 (1973).
[39]J. R. Haynes, Phys. Rev. Lett. **4**, 361 (1960).
[40]P. G. Lagoudakis, M. D. Martin, J. J. Baumberg, G. Malpuech, and A. Kavokin, J. Appl. Phys. **95**, 2487 (2004).
[41]K. Kojima, M. Funato, K. Kawakami, S. Nagahama, T. Mukai, H. Braun, and U. T. Schwarz, Appl. Phys. Lett. **89**, 241127 (2006).
[42]D. Hirano and Y. Kanemitsu, J. Lumin. **128**, 712 (2008).
[43]R. H. Dicke, Phys. Rev. **93**, 99 (1954).
[44]K. V. Kavokin, M. A. Kaliteevski, R. A. Abram, A. V. Kavokin, S. Sharkova, and I. A. Shelykh, Appl. Phys. Lett. **97**, 201111 (2010).
[45]B. Rau, P. Waltereit, O. Brandt, M. Ramsteiner, K. H. Ploog, J. Puls, and F. Henneberger, Appl. Phys. Lett. **77**, 3343 (2000).
[46]Y. J. Sun, O. Brandt, M. Ramsteiner, H. T. Grahn, and K. H. Ploog, Appl. Phys. Lett. **82**, 3850 (2003).
[47]P. Corfdir, P. Lefebvre, J. Ristic, P. Valvin, E. Calleja, A. Trampert, J.-D. Ganière, and B. Deveaud-Plédran, J. Appl. Phys. **105**, 013113 (2009).
[48]P. Corfdir (private communication).